Testing of a Novel Induction Heat Treated Steel Brace with Enhanced Buckling Behaviour

Jamshiyas, Shadiya; Skalomenos, Konstantinos

DOI:
10.1002/cepa.2581

Document Version
Publisher's PDF, also known as Version of record

Citation for published version (Harvard):
Jamshiyas, S & Skalomenos, K 2023, 'Testing of a Novel Induction Heat Treated Steel Brace with Enhanced Buckling Behaviour', *ce/papers*, vol. 6, no. 3-4, pp. 908-913. https://doi.org/10.1002/cepa.2581

ce/papers Proceedings in civil engineering

Ernst & Sohn A Wiley Brand

ORIGINAL ARTICLE

eurosteel AMSTERDAM 2023

Ernst & Sohn A Wiley Brand

Testing of a Novel Induction Heat Treated Steel Brace with Enhanced Buckling Behaviour

Shadiya Jamshiyas[1]| Konstantinos Skalomenos[1]

Correspondence

Dr. Konstantinos Skalomenos
Dept. of Civil Engineering
University of Birmingham
United Kingdom
B15 2TT
Email: k.skalomenos@bham.ac.uk

[1] Department of Civil Engineering, University of Birmingham, Birmingham, United Kingdom

Abstract

Steel braces are widely used to stabilize steel structures forming horizontal or vertical truss structures; however, their relatively poor buckling behaviour is often lead to overdesigned structures. Induction Heat (IH) treatment technology is a novel contactless material transformation process to effectively strengthen local areas of steel sections. Utilizing IH to increase the strength of the middle length of steel brace sections, buckling behaviour can be improved. The present study experimentally investigates the compression behaviour of the novel braces fabricated by IH-treated circular hollow steel sections. A Digital Image Correlation (DIC) system is used to measure the experimental deformation quantities, such as axial displacements, out-of-plane deformations, and strain distributions along the brace length. Four specimens were tested with two set of different slenderness ratios (λ). Each set includes one conventional steel brace (CSB) and one IH-treated steel brace (IHSB) with a stronger section at its mid-length. The specimens were subjected to a monotonic displacement-controlled loading history until reaching an axial compressive strain of 2.5%. It was found that buckling load can increase up to 20% in IHSBs. IH treatment was also beneficial in improving the post-buckling behaviour of the brace. The compression strength was found to be more than double in IHSBs than in CSBs at a ductility level of 5 (ductility is defined as the ratio of the target axial displacement to the yielding axial displacement). Moreover, out-of-plane displacements were reduced by 28% for the IHSBs at an axial strain of 1% showing a more evenly distribution of strain demands along the brace length.

Keywords

Steel braces, buckling, induction heating, strengthening, digital image correlation (DIC) system, displacement-controlled loading, circular hollow sections.

1 Introduction

Steel braces are critical structural elements which contribute to the distribution of loads in structures by providing strength and stiffness. Although a range of bracing systems have been developed over the last years, the instability phenomenon of buckling has restricted the utilization of their full potential under compressive loads [1]. Buckling causes the member to deform laterally and results in a sudden loss of its load carrying capacity.

Researches have been constantly carried out to address the failure of steel structures through buckling. Most of the methods currently employed to improve the buckling capacity of steel members adopt a composite design strategy involving altered section profiles and characteristics. Current techniques used in the industry are application of steel plates to the exterior through welding [2], application of carbon fibre reinforced polymers sheets (CFRPs) [3] and use of concrete-filled steel tubes (CFST) [4]. Whilst these applications boast a significant enhancement to the buckling performance, they possess many downfalls, most notably the increased dead weight of the structure, debonding of CFRPs and debonding of concrete from steel casing due to temperature effects.

Recently, with an aim to overcome these shortcomings, an innovative method of increasing the yielding stress of steel members locally through induction heating (IH) has been explored [5]. The IH is a material transformation process that can increase the strength of steel at a critical location by forming a refined martensite. During the manufacturing process, the selected area of the steel workpiece is heated up to high temperatures (~900°) and then it is immediately cooled down by water, i.e., quenching. The advantages of IH are energy efficiency, speed, safety, cleanliness, accuracy, and repetition [6]. This approach may offer an economical mean of improving buckling resistance of steel braces while maintaining standardized steel profiles.

https://doi.org/10.1002/cepa.2581 wileyonlinelibrary.com/journal/cepa

2 Brace: Concept and Deformation Mechanism

In the proposed brace concept, the middle section has higher strength than the section near the brace ends, as shown in Fig. 1. While the section at brace ends maintains the yield stress of conventional steel, σ_{yCS}, the middle section achieves a 2-3 times higher yield stress than σ_{yCS} through IH treatment. This creates a boundary between the IH treated steel and conventional steel (CS), where a distinct transition in material strength occurs. Under this design, the steel brace exhibits a new deformation mechanism under compression. Strain concentrates along the untreated portions of the brace keeping the middle section elastic. This may help the brace member to reach σ_{yCS} before buckling occurs, thus increasing the compression strength of the member. For a given axial deformation, the lateral deflections decreases and the post-buckling strength increases.

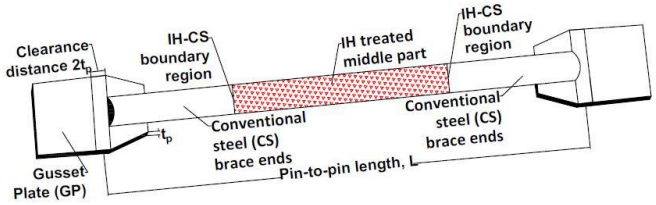

Figure 1 Brace with IH treatment in the middle.

Conventional Steel Braces (CSB) under compressive loads exhibit symmetrical buckling by forming a plastic hinge in the middle section. In case of IH-treated Steel Braces (IHSB), either a symmetrical or an asymmetrical buckling behaviour may be observed. When symmetrical buckling occurs, the plastic hinge is formed in the middle section, similar to CSB. In asymmetrical buckling the plastic hinge is formed at the brace ends, near the IH-CS material boundary, as shown in Fig. 2.

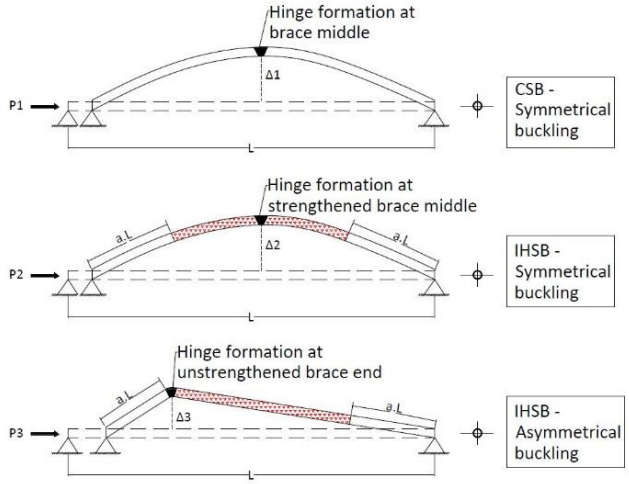

Figure 2 A schematic representation of the buckling mechanism in CSB and IHSB.

In Fig. 2, *P1*, *P2* and *P3* are the buckling loads of CSB, IHSB-symmetrical, and IHSB-asymmetrical, respectively. $\Delta 1$, $\Delta 2$ and $\Delta 3$ denote the corresponding out-of-plane displacements, *L* is the total length of the brace and *a.L* is the untreated length at brace ends for the IHSBs. Buckling behaviour in IHSBs is controlled by the slenderness ratio, the yielding stress ratio between IH-steel and conventional steel (IH/CS ratio), and geometrical imperfections.

Considering the bending moment induced by the axial force *P* in Fig. 2, the equilibrium of forces requires that:

$$\frac{P}{A} + \frac{P \cdot \Delta}{S} = \sigma_{max} \qquad (1)$$

where $\Delta = \frac{1}{1-\frac{P}{P_{cr}}} \Delta_0 \sin \pi x/L$ (2)

Here *P* is the maximum axial load limited by buckling, *A* is the area of cross-section, Δ is the out-of-plane displacement (lateral deflection), *S* is the elastic section modulus, σ_{max} is the maximum compressive stress in the outermost fibre of the steel section, P_{cr} is the Euler's critical buckling load, Δ_0 is the initial deformation along the brace length, *x* is the distance at which buckling happens/ hinge formation occurs and *L* is the total length of the brace.

In case of CSB and IHSB-asymmetric, the σ_{max} is limited by the yield stress of the untreated steel section, σ_{yCS}, while in case of IHSB-symmetric, σ_{max} is limited by the yield stress of IH-treated middle section, σ_{yIH}. Thus, by utilizing Eq. (1) and (2) we can define:

In CSB $$\frac{P1}{A} + \frac{P1 \cdot \Delta_0 \sin \pi x/L}{S \cdot (1-\frac{P1}{P_{cr}})} = \sigma_{yCS}$$

where $x = 0.5L$ (3)

In IHSB-symmetrical $$\frac{P2}{A} + \frac{P2 \cdot \Delta_0 \sin \pi x/L}{S \cdot (1-\frac{P2}{P_{cr}})} = \sigma_{yIH}$$

where $x = 0.5L$ (4)

In IHSB-asymmetrical $$\frac{P3}{A} + \frac{P3 \cdot \Delta_0 \sin \pi x/L}{S \cdot (1-\frac{P3}{P_{cr}})} = \sigma_{yCS}$$

where $x < a.L$ (5)

From Eq. (3) and (4), $\sigma_{yCS} < \sigma_{yIH}$, therefore, $P1 < P2$.
From Eq. (2), (3) and (5), $\Delta_1 > \Delta_3$ *as 'x'* value differs in CSB and IHSB-asymmetrical. As σ_{max} is the same for both cases, we conclude that $P1 < P3$. It is obvious from the above that IHSB may exhibit a higher compressive strength than CSB for all cases.

3 Experimental Study

3.1 Overview of the Test Specimens

Four brace specimens with gusset plate (GP) connections are fabricated at a ¼ - scale. Two different cross-sections have been used, one section has diameter of 48.3 mm and thickness of 3.2mm (48.7 x 3.2mm), while the other section has a diameter of 33.7 x and thickness of 3.2mm (33.7 x 3.2mm). All specimens are configured by hot finished circular hollow sections made of grade S355. The gusset plates are fabricated using S355 plates of 9mm and 6mm thickness, respectively. The specimens are designed according to EN 1993 and AISC/ANSI 360 [7, 8]. The treatment length in IHSBs is equal to '0.75L', where *L* is the pin-to-pin length of the specimen. The specimens are manufactured to act as pin-ended members by providing a clearance distance (unrestrained region) equal to $2t_p$

within the vicinity of gusset plates (t_p is the thickness of the gusset plate), as shown in Fig. 1. This enables a "free" rotation of brace ends [9]. After buckling initiation, a hinge is formed within the clearance distance. The slenderness ratio (λ) of the specimens is 43 (L = 700 mm) for the section 48.7 x 3.2mm and 73 (L = 800 mm) for the section 33.7 x 3.2mm. The characteristics of the test specimens are listed in Table 1.

Table 1 Specifications of test specimens

Specimen Category	Diameter (ϕ) x Thickness (t) x pin-pin length (L)(mm)	IH treated length in the brace middle, 0.75L(mm)	Gusset plate thickness, t_p (mm)	Slenderness, λ
CSB-43	48.3 x 3.2 x 700	-	9	43
IHSB-43	48.3 x 3.2 x 700	525	9	43
CSB-73	33.7 x 3.2 x 800	-	6	73
IHSB-73	33.7 x 3.2 x 800	600	6	73

3.2 Material Properties

Tensile coupon tests are carried out according to the ASTM standards A-370 [10] to determine the material properties of the circular hollow sections and steel plates used for the manufacturing of the brace specimens. The material properties are tabulated in Table 2 and the engineering stress-strain curves are presented in Fig. 3.

Table 2 Material data from coupons

Material	Thickness, t (mm)	Young's Modulus, E (MPa)	Yield Strength, σ_y (Mpa)	Ultimate Strength, σ_u (Mpa)	% Elongation at UTS	% Elongation after Fracture
CS	3.2	202647	365.9	501.8	13.3	19.2
IH	3.3	229510	849.2	994.7	3.6	8.1
GP-6	6	180773.3	444.3	555.2	13.1	20.3
GP-9	9	184953.5	414.2	567.9	12.3	20.4

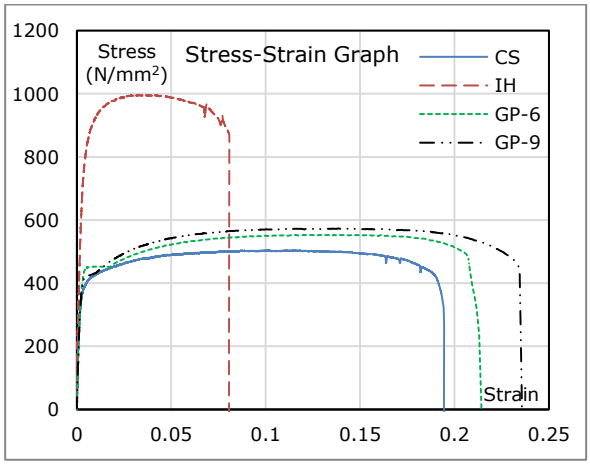

Figure 3 Stress-strain curves of the materials used.

3.3 Test Set-up and Measurement System

The loading frame for the specimen is designed with a rigid foundation beam and a sturdy jack connector affixed to the actuator head, as shown in Fig. 4. The specimen is then placed axially within this set-up and bolted to the bottom steel beam and to the jack connector on the top. The measurement system consists of a Digital Image Correlation (DIC) system, four strain gauges mounted along the length of the specimen and two strain-gauge type displacement transducers attached to either side of the specimen (the average value is taken as the total axial displacement).

DIC is an advanced digitalized method to measure displacements and strain quantities over a material tested, by tracking a unique distribution of pixel intensities of a grey scale image called a pattern or template [11]. The cameras detect the measuring surface by identifying a black dot pattern painted on white background. The cameras are connected to a computer and server system managed through a software. Post-processing of the images recorded gives the required response quantities. Fig. 4 shows an overview of the measurement system.

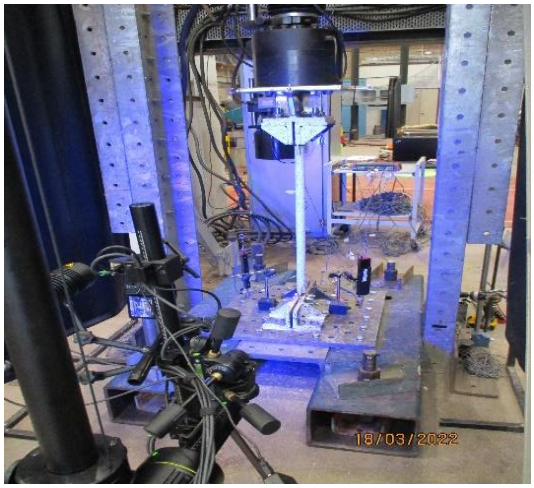

Figure 4 Experimental setup and measurement system.

4 Results and Discussions

4.1 Compression Test Results

A monotonic displacement-controlled loading history is applied to the specimens using an actuator of capacity 500kN up to an axial strain level of 2.5% (axial displacement 20mm). Fig. 5 shows the overall deformation of the specimens at this strain level. One can observe from this figure the formation of plastic hinge at the critical location of buckling. CSB buckled symmetrically as expected forming a plastic hinge in the mid-length. It is noteworthy that IHSB-43 exhibited asymmetrical buckling and IHSB-73 symmetrical buckling. Table 3 lists important response quantities such as the buckling load and axial strain at which global buckling occurred in each specimen. Comparison of normalized force – displacement curves are presented in Fig. 6. In this figure, x-axis is the axial strain and y-axis is the normalized load, P/P_y. Note P_y is the yielding load based on DIC measurements.

(a) CSB-43

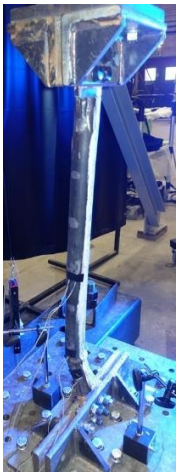

(b) IHSB-43

(c) CSB-73

(d) IHSB-73

Figure 5(a-d) Overall bucking mechanism of specimens at 2.5% axial strain level.

Table 3 Compression test details

Type	Buckling Load (kN)	Axial Strain at buckling (%)
CSB–43	214.7	-0.72
IHSB-43	188.5	-0.96
CSB–73	80.4	-0.19
IHS -73	95.5	-0.35

From the compression test results detailed in Table 3 and shown in Fig. 6(a-b), IHSB shows a clear dominance over CSB in terms of buckling strength for both slenderness ratios. There is an increase of buckling load by 14% for IHSB over CSB in case of asymmetrical buckling and by 20% in case of symmetrical buckling. The axial strain at which buckling occurred is higher for IHSB compared to CSB at both slenderness ratios. Even though the strain demand is higher in the conventional steel part for the IHSB for a given axial strain, the brace resisted buckling until a larger axial strain than CSB, as shown in Table 3. Fig. 6(a-b) also compares the normalized *P1, P2* and *P3* calculated by Eqs. (3), (4) and (5), respectively, with the test values. Part of the difference between calculated and experimental strength is probably because of the gusset plate restraint which is ignored in the present set of equations.

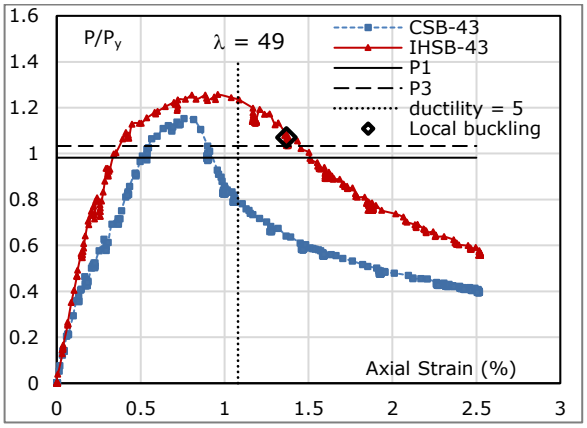

(a) λ = 43

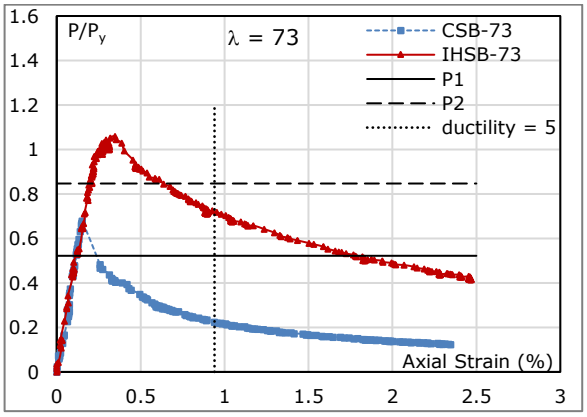

(b) λ = 73

Figure 6(a-b) Normalized force-displacement curve for the test specimens.

In Fig. 6a, where asymmetrical buckling occurred for the IHSB-43, one can observe a slight difference in elastic stiffness between the IHSB-43 and the CSB-43. This is likely due to the flexural component of the elastic response that might be larger in the CSB-43 than in the IHSB-43. Note that yielding is developed towards the brace ends in asymmetrical buckling and flexural deflection is smaller compared to symmetrical buckling, thus providing higher elastic stiffness. In Fig. 6b, such a difference in stiffness was not observed, perhaps because buckling was symmetrical for both the CSB-73 and IHSB-73 specimens. As shown in Fig. 6a, local buckling initiated in IHSB-43 near an axial strain of 1.4%. Note that no local buckling was observed in the rest specimens.

4.2 DIC Results

DIC data can provide a clear picture about the strain distribution and out-of-plane deformation along the length of the specimen at specific locations such as in brace ends, IH-CS boundaries, and middle section of the brace. The yielded areas in the specimens are identified by calculating the yield displacement for both CS and IH steel and comparing it with the strain values at the critical locations during different stages of the test. The strain distribution along the length of the specimens at 2% axial strain level are shown in Fig. 7. The calculated yield strain for CS (0.188%) and for IH steel (0.400%) are represented as minimum and maximum values respectively, in the scale shown in the Fig. 7.

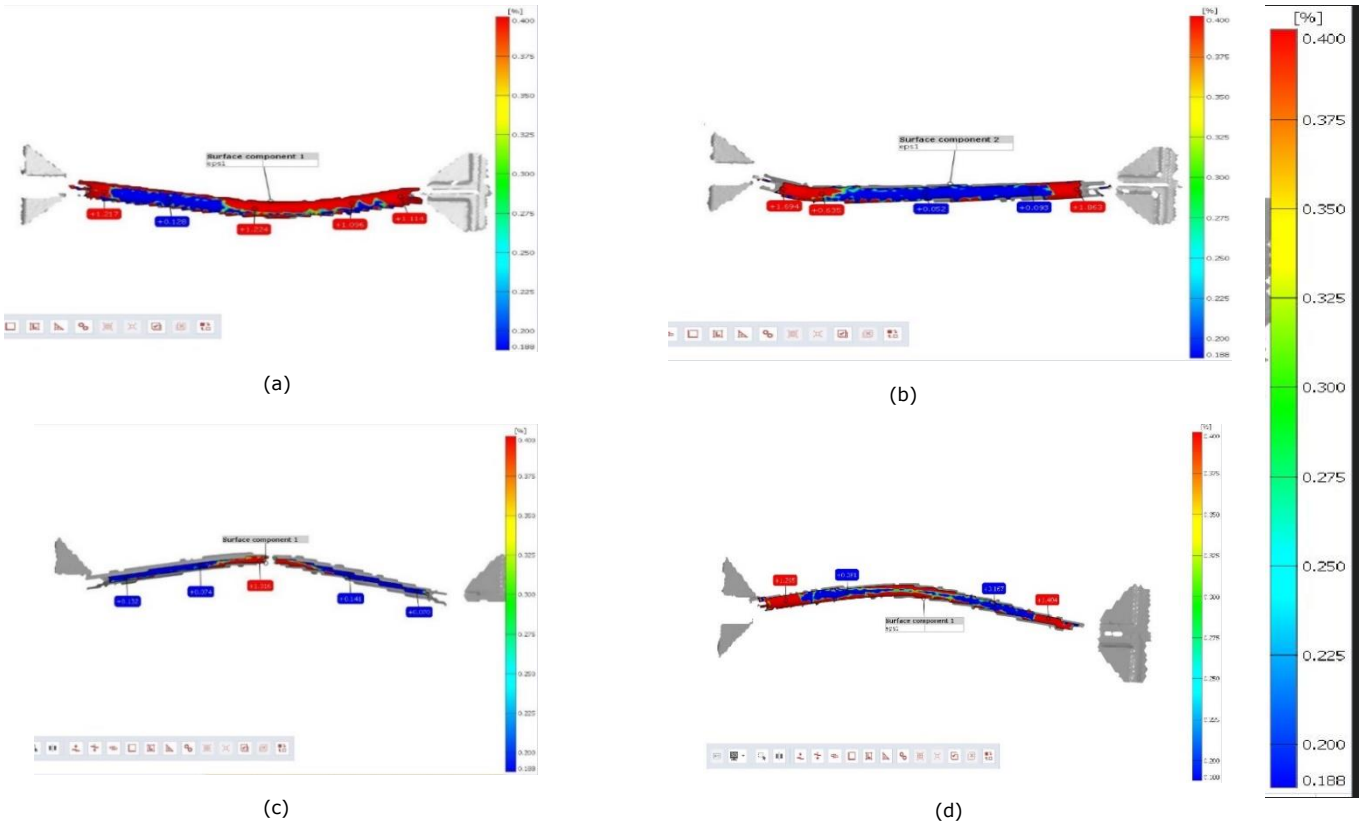

Figure 7 Strain distribution along the length of the brace at 2% axial strain level: (a) CSB-43; (b) IHSB-43; (c) CSB-73; (d) IHSB-73.

Fig. 7(a-d) illustrates the yielding mechanism of CSB and IHSB specimens. While CSB yielded in the brace middle, IHSB first yielded at the conventional steel portions of brace ends, keeping the brace middle elastic. This proves the effectiveness of the proposed member design and its novel yielding mechanism. For the case of symmetrical buckling, strains are distributed within the two pre-designed yielding zones instead of one location (i.e., brace middle), thereby ensuring a more uniform absorption of the deformation.

Fig. 8 shows the out-of-plane deformation as measured along the brace length at 1% axial strain. The location of plastic hinge for each specimen is marked by red circles in this figure. In Fig. 8(a) and (b), Δ was found to be smaller for the IHSB compared to the CSB for both buckling mechanisms. By strengthening the middle section of the brace, out-of-plane deformations can be reduced, thus providing a greater stability.

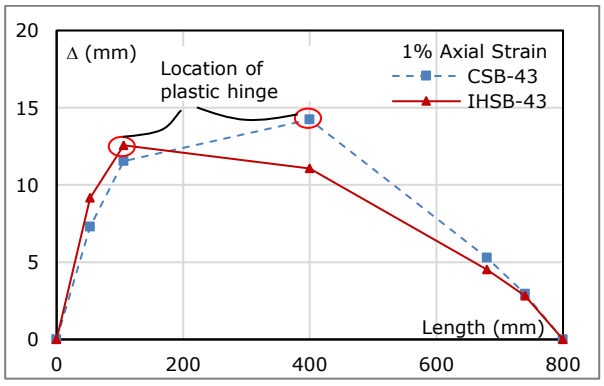

(a) λ = 43

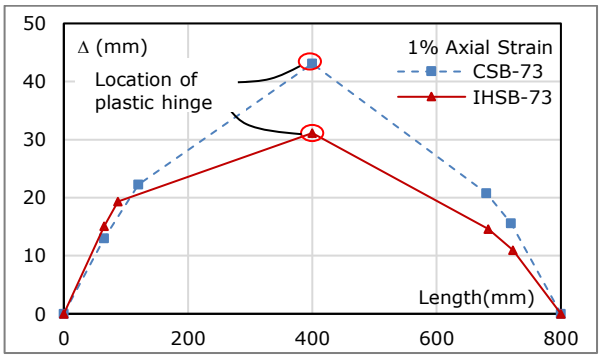

(b) λ = 73

Figure 8(a-b) Out-of-plane deformation at critical locations of the brace specimens at 1% axial strain level.

4.3 Post-buckling compressive resistance

A significant increase of the post-buckling strength can also be observed for the IHSBs compared to CSBs, as shown in Fig. 6. Looking into the post-buckling strength at different ductility levels someone can assess the drop of the compressive strength under large deformations. Similar to the study conducted by Tremblay [12], the post-buckling resistance for the tested specimens are considered for a chosen ductility level of 5. The ductility, $\mu = \delta/\delta_y$ (calculated as ratio of target displacement to yield displacement), where δ_y is the yield displacement, calculated as $\varepsilon_y \times L$ where $\varepsilon_y = \sigma_y/E$. σ_y is the yield stress and E is the Young's modulus. The yielding displacement for all specimens is found to be 1.51mm and ductility 5 corresponds to an axial displacement equal to 7.5mm.

At this ductility level, the post-buckling strength of the

IHSB-43 and IHSB-73 is found to be 1.35 and 3.2 times higher than that of the CSB-43 and CSB-73, respectively. At this high level of inelastic deformations, axial strength of the brace is mainly defined by the hinge flexural strength and the hinge location (P-Δ effect). For the case of IHSB-43, a plastic hinge is formed near the brace ends where lateral deformations (Δ) are smaller than those of CSB-43. This naturally increases the compressive strength P. For the case of CSB-73 and IHSB-73, a plastic hinge is formed at the middle of the specimens, but IHSB-73 middle section enjoys higher plastic moment thanks to IH steel. In addition, Δ is found to be smaller for IHSB-73 which further increased P. It should be noted that IH treatment was found to be more effective for the higher slenderness specimen. IHSB-43 experienced local buckling within the plastic hinge due to a relatively high concentration of strains along the untreated portions of the brace (brace ends). This caused a slightly steeper decrease of the post-buckling strength in IHSB-43 compared to IHSB-73, as shown in Fig. 6. A longer untreated length might be effective in delaying the initiation and the growth of local buckling. DIC data was found to be very efficient for assessing the new yielding and buckling mechanisms of IHSB specimens.

Conclusions

A novel steel brace, namely IHSB, is proposed to enhance the poor buckling behaviour of conventional steel braces (CSB). Based on an experimental study, the main conclusions are as follows:

- IHSB showed an enhanced buckling behaviour compared to CSB. Buckling load and post-buckling strength increased up to 20% and more than 33%, respectively.
- IHSB may exhibit an asymmetrical or symmetrical buckling behaviour depending on its slenderness ratio. A change in bucking behaviour from asymmetrical to symmetrical was observed when the slenderness ratio increased from 43 (IHSB-43) to 73 (IHSB-73).
- Even though the strain demand is higher in the conventional steel part for IHSB, the novel brace could resist buckling until a larger axial strain than CSB. There is an increase of 33% in the axial strain at buckling for the IHSB-43 and an increase of 84% for the IHSB 73.
- At 1.4% axial strain, IHSB-43 experienced local buckling within the area of the plastic hinge. This caused a slightly steeper decrease of the post-buckling strength in IHSB-43 compared to the IHSB-73. No local buckling was observed in the rest specimens.
- The Digital Image Correlation (DIC) system appeared to be a valuable measurement system for conducting a comprehensive analysis of various aspects of the inelastic response of the novel brace. DIC was efficient to accurately analyse the new yielding and buckling mechanism, identify critical plastic zones and measure out-of-plane deformations.

Acknowledgements

The project has been supported by The Royal Society Research Grant, United Kingdom (RGS\R1\211310). Additionally, the authors would also like to acknowledge the School of Engineering at the University of Birmingham who collectively supported this project.

References

[1] Borthakur D.J.; Chetia, N. (2016). *A study on the effectiveness of bracing system for lateral loading*. International Journal of Advanced Engineering Research and Science 2016, 3, p. 4.

[2] Gurney, T. R.; Madox, S. J. (1972). *Determination of fatigue design stresses for welded structures from an analysis of data*. Metal construction and British Welding Journal 1972, 4, p. x-5.

[3] Shaat, A.; Fam, A. Z. (2009). *Slender steel columns strengthened using high-modulus CFRP plates for buckling control*. Journal of Composites for Construction 2009, 13, p. 2-12.

[4] Gupta, P. K.; Sarda, S. M.; Kumar, M. S. (2007). *Experimental and computational study of concrete filled steel tubular columns under axial loads.* Journal of Constructional Steel Research 2007, 63, p. 182-193.

[5] Skalomenos, K.A.; Kurata, M.; Fukutomi, Y.; Nishiyama, M (2018). *Analytical and experimental study on steel braces with stronger middle length treated by induction hardening*. Eleventh U.S. National Conference on Earthquake Engineering**,** Integrating Science, Engineering & Policy 2018, Los Angeles, California.

[6] Skalomenos, K.A.; Kurata, M.; Shimada, H.; Nishiyama, M (2018). *Use of induction-heating in steel structures: Material properties and novel brace design*. Journal of Constructional Steel Research 2018, 148, p. 112-123.

[7] EN 1993-1-8 (2005). *Eurocode 3: Design of steel structures – Part 1-8: Design of joints*. May 2005.

[8] ANSI/AISC 360-16 (2016). *Specifications for structural steel buildings*. July 2016.

[9] Skalomenos, K.A.; Kurata, M.; Nakashima, M. (2018). *Seismic Capacity Quantification of Gusset-Plate Connections to Fracture for Ductility-Based Design*. Journal of Structural Engineering 2018, 10, p. 04018195: 1-13.

[10] ASTM A370 / ASME SA-370 (2019). *Standard Test Methods and Definitions for Mechanical Testing of Steel Products*. July 2019.

[11] Arola, A.M et al. (2019). *Digital image correlation and optical strain measurement in bendability assessment of ultra-high strength steels*. Procedia Manufacturing 2019, 29, p. 398-405.

[12] Tremblay, R (2002). *Inelastic Seismic Response of Steel Bracing Members*. Journal of Constructional Steel Research 2002, 58, p. 665-701.